

Multiband tight-binding model of local magnetism in $\text{Ga}_{1-x}\text{Mn}_x\text{As}$

Jian-Ming Tang and Michael E. Flatté

Department of Physics and Astronomy, University of Iowa, Iowa City, IA 52242-1479

We present a theoretical approach to $\text{Ga}_{1-x}\text{Mn}_x\text{As}$ that captures much of the physics neglected in effective mass theories but remains computationally tractable. The GaAs host is described by a sp^3 tight-binding Hamiltonian that incorporates spin-orbit interaction, and the Mn impurity is described by a local p - d hybridization and on-site potential. Local spin-polarized resonances within the valence bands significantly enhance the local density of states (LDOS) near the band edge, which is consistent with angle-resolved photoemission and magnetoabsorption measurements, but is not contained in effective mass theories. We present the spin and orbitally resolved LDOS for a single Mn impurity in the GaAs host as well as for two interacting Mn impurities. The acceptor states hybridize and split in energy when two Mn magnetic moments are parallel. The splitting of the acceptor level is anisotropic and exceeds 10 meV even if the Mn impurities are separated by as many as 20 Å. This suggests that scanning tunneling spectroscopy can directly measure the Mn-Mn interaction energy as a function of distance.

PACS numbers: 75.50.Pp, 75.30.Hx, 75.30.Gw, 71.55.-i

The successful growth of ferromagnetic diluted magnetic semiconductors (DMSs) based on III-V compounds [1, 2, 3, 4, 5] has attracted much attention due to the nearby metal-insulator transition and also for their potential application to nano-scale nonvolatile storage devices and to quantum computation [6, 7]. In order to turn a nonmagnetic semiconductor into a magnet, a sizable amount ($\sim 1\%$) of magnetic dopants are introduced. Experimental studies [2, 8, 9, 10, 11, 12] have shown strong correlations between the ferromagnetism and the hole carriers that are also contributed by the Mn doping in the III-V DMSs. The emerging picture of this ferromagnetism is that the Mn magnetic moments are localized, and the ferromagnetic coupling is mediated through the delocalized hole carriers [6, 13]. A deeper understanding of this ferromagnetic coupling has been hampered by insufficient knowledge of the valence band structure. The assumption that the holes reside in the unperturbed valence bands of the host semiconductors [2, 8, 14] has recently been questioned by both theoretical and experimental studies [10, 12, 15, 16]. Effective mass theories provide good spectral resolution at the band edge, but cannot describe distortions on distances of one or two lattice constants for they are only accurate for momenta close to the Γ point. Density functional calculations [17, 18], however, describe local properties well, but state of the art supercell calculations have not had sufficient spectral resolution to resolve the shallow bound states in the gap and the sharp resonances in the valence bands.

In this Letter we study the local density of states (LDOS) of very dilute concentrations of Mn in GaAs as a prototype III-V DMS, and show that the valence bands are strongly altered by the Mn dopants, and in return influence the interaction between the Mn magnetic moments. In order to obtain both sufficient spectral resolution and proper dispersion relations throughout the full

Brillouin zone, a multiband tight-binding approach incorporating spin-orbit interaction is employed. Our results show that the hybridization between the Mn 3d-orbitals and the GaAs valence bands leads to spin-polarized resonances *within the valence bands* and to delocalized ferromagnetic interaction. The LDOS near the valence band edge is significantly enhanced by these resonances. Each Mn dopant can enhance the LDOS by as much as a factor of 2 up to the second-nearest neighbors (See Fig. 1), corresponding to a $\sim 7\%$ increase of the average LDOS for 1% Mn concentration. The strong LDOS enhancement is consistent with recent angle-resolved photoemission measurements [16], and qualitatively explains the increases of the absorption coefficients in the intraband [12] as well as the interband absorption spectroscopies [9, 10]. In particular, the experimental result that the band-edge absorption coefficient increases in finite magnetic fields more for one polarization of light is consistent with our result that the resonances are both orbitally- and spin-polarized.

Whereas the spin-polarized band-edge resonances will alter the Mn-Mn interaction, the acceptor states provide a direct means of measuring that interaction. The acceptor level of Mn splits when two Mn magnetic moments are in a parallel configuration [19]. The range of interaction between the Mn dopants can be probed by the size of the splitting as a function of the separation. We find that the splittings are as large as tens of meV even when two Mn dopants are separated by a few lattice constants. This magnetic interaction is anisotropic with respect to the axis connecting the two Mn dopants due to spin-orbit interaction, in qualitative agreement with the continuum model [20]. Both the local enhancement of the valence band edge and the splitting of the acceptor level could be probed by scanning tunneling spectroscopy (STS) [21].

The intriguing character of Mn-doped III-V DMSs originates in the dual nature of the coupling between

the Mn 3d-orbitals and the neighboring dangling sp^3 -hybrids. As pointed out by Vogl and Baranowski [22], the fivefold degenerate 3d-orbitals split in a cubic lattice to an E -symmetric ($d_{x^2-y^2}$ -like) doublet, which is only weakly coupled to the tetrahedral host, and a T_2 -symmetric (d_{xy} -like) triplet, which can effectively couple to the sp^3 -hybrids. The antibonding states of the T_2 -symmetric states and the sp^3 -hybrids form the acceptor states within the gap. These antibonding states are delocalized in space since they overlap strongly with the host valence bands. In our calculations the above features show up in the following way. The hybridization of the majority Mn d-orbitals is treated as an effective extended spin-dependent potential U_1 acting on the four nearest-neighbor sites of Mn, because only s and p orbitals are explicitly used in our tight-binding Hamiltonian. The operator form of our Mn potential is

$$V = U_0 \sum_{\ell,s} c_{\ell s}^\dagger(\mathbf{R}_0) c_{\ell s}(\mathbf{R}_0) + U_1 \sum_{j=1}^4 \sum_{\ell} c_{\ell \uparrow}^\dagger(\mathbf{R}_j) c_{\ell \uparrow}(\mathbf{R}_j), \quad (1)$$

where U_0 is the on-site orbital energy difference, $c_{\ell s}^\dagger(\mathbf{R})$ ($c_{\ell s}(\mathbf{R})$) is the creation (annihilation) operator of a spin- s electron in the ℓ orbital at site \mathbf{R} . The Mn dopant is located at \mathbf{R}_0 , and the four nearest-neighbor sites are labeled by \mathbf{R}_1 - \mathbf{R}_4 . We neglect the difference of the potential matrix elements between the s and p orbitals, because the s -orbitals make a negligible contribution to the LDOS near the valence band edge. The quantization axis for the spin is aligned with the Mn core spin. The minority Mn d-orbitals are assumed to be much higher in energy, and the hybridization energy of them with the spin-down states is neglected. We find that the effective potential U_1 is of critical importance in inducing the acceptor level at the experimentally observed energy. The significance of the hybridization to the acceptor level energy has also been noted recently by Dietl *et al.* [23]. As for the delocalized nature of the acceptor state, our results show that only about 10% of the spectral weight of the acceptor state is concentrated at the Mn site, 20% is distributed over the four nearest-neighbor sites, and the remaining 70% is extended to farther sites. Furthermore, the large spin-orbit interaction of GaAs splits the gap states into three different energy levels, and introduces anisotropy to the spatial structure.

We use the Koster-Slater technique [24] to calculate the Green's function whose imaginary part gives the LDOS. This method has been proven to give the correct chemical trend of impurity levels in semiconductors [25], and we have previously applied it to successfully predict STM spectra near impurities in superconductors [26]. Starting with the tight-binding Hamiltonian $\hat{H}_0(\mathbf{k})$ of homogeneous GaAs, one first calculates the retarded Green's function, $\hat{G}_0(\mathbf{k}, \omega) = [\omega - \hat{H}_0(\mathbf{k}) + i\delta]^{-1}$. To obtain a good description of the valence band structure, we

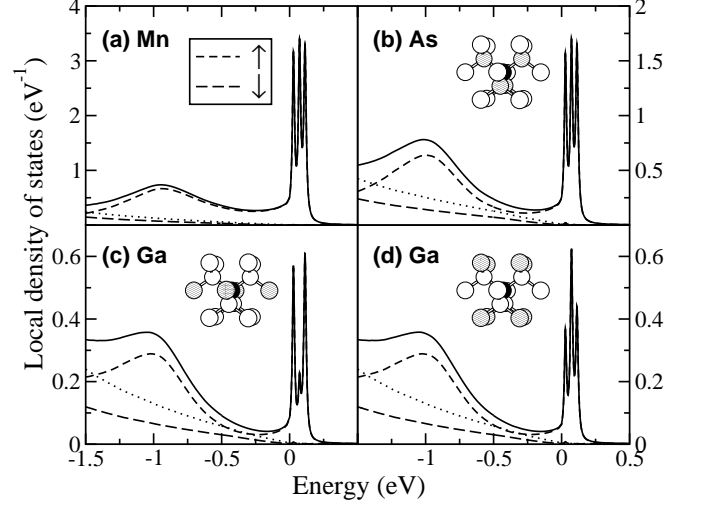


FIG. 1: LDOS spectra for the charged (ionized) Mn dopant in $\text{Ga}_{1-x}\text{Mn}_x\text{As}$ (corresponding to bulk n -doped) at (a) the Mn site, at (b) one of the nearest-neighbor As sites, and at (c and d) one of the second-nearest-neighbor Ga sites. The shaded balls in each panel show the corresponding atomic sites, and the black ball shows the Mn site. The Mn core spin is aligned with the z -axis of the lattice, and the z -axis is aligned vertically. In this particular case, the spectra at four nearest-neighbor sites are identical, and have two different functional forms at the second-nearest-neighbor sites. The total LDOS is shown by the solid lines. The dashed lines show the projections onto the two spin polarizations relative to the Mn core spin. The dotted lines show the LDOS of the bulk GaAs. The zero of energy is the valence maximum of bulk GaAs. The valence band LDOS of bulk GaAs is more concentrated at the As sites than at the Ga sites, because the LDOS is the density of states modulated by the probability density of electrons. For the neutral Mn dopant (corresponding to bulk p -doped $\text{Ga}_{1-x}\text{Mn}_x\text{As}$) only the highest energy peak of the three localized peaks apparent above in each panel would be visible.

use the sp^3 model including spin-orbit interaction [27]. Then, by Fourier transforming $\hat{G}_0(\mathbf{k}, \omega)$, we construct the homogeneous Green's function in coordinate space, $\hat{G}_0(\mathbf{R}_i, \mathbf{R}_j, \omega)$, where \mathbf{R}_i and \mathbf{R}_j label the zincblende lattice sites. This step consumes the majority of computation time. It takes about one day for one link ($\mathbf{R}_i - \mathbf{R}_j$) with a spectral range of 2 eV on a personal computer. The number of links used in this study is about 500. A constant linewidth of $\delta = 10$ meV produces a good spectral resolution within a reasonable computation time. The final Green's function is obtained by solving the Dyson's equation,

$$\check{G}(\omega) = \check{G}_0(\omega) + [\check{1} - \check{G}_0(\omega)\check{V}]^{-1} \check{G}_0(\omega), \quad (2)$$

where $\check{G}(\omega)$ is the full matrix representation using all atomic orbitals at all lattice sites. The LDOS at each site \mathbf{R}_i is given by

$$A(\mathbf{R}_i, \omega) = -\frac{1}{\pi} \text{Im} \left[\text{tr}_\alpha \hat{G}(\mathbf{R}_i, \mathbf{R}_i, \omega) \right], \quad (3)$$

where the tr_α is taken with respect to the orbitals of the α atom, depending on which type of atom is actually located at the site \mathbf{R}_i .

To determine the values of U_0 and U_1 , we first consider the possibility that the potential is nonzero only at the Mn site ($U_1 = 0$), and the size of the on-site potential is assumed to be the same for all orbitals. When the Mn atom replaces a Ga atom, the strength of this on-site potential is estimated to be $U_0 \sim 1$ eV based on the energy difference of the ionization energies of Ga ($4s^24p$) and of Mn ($3d^54s4p$), which are about 6 and 5 eV respectively. The Mn atom has lower ionization energy, and, therefore, is attractive to holes. Not only is this on-site potential too weak to bind any acceptor level in the gap, it is not possible (even with an unrealistically large on-site potential, $U_0 \gg 10$ eV) to bind a hole more than 60 meV above the valence band edge. The Mn dopant introduces an acceptor level at 113 meV above the valence band edge, therefore, the effective potential must be extended at least to the four nearest-neighbor As sites. If we fix $U_0 = 1$ eV, and tune U_1 to give the correct acceptor level energy, the required nearest-neighbor potential is about 3.59 eV. This nearest-neighbor potential is too large to be accounted for by the tail of the screened Coulomb potential. The screened Coulomb potential at the nearest-neighbor sites of a singly charged Mn center is only about 0.5 eV, or even smaller if the system is doped with carriers, as in our case. Therefore, the large effective potential at the nearest-neighbor sites must result from the hybridization of the Mn $3d$ -orbitals and the host sp^3 -hybrids as in the picture of Vogl and Baranowski [22]. The exchange interaction effectively pushes the valence-band states with the same spin polarization as the Mn core spin into the gap. The states with the opposite spin polarization essentially remain unperturbed, because it is energetically unfavorable to fill an electron into Mn $3d$ -orbitals with an opposite spin. The final values of the matrix elements of the Mn potential are $U_0 = 1$ eV and $U_1 = 3.59$ eV.

Figure 1 shows the LDOS spectra at the Mn site and at neighboring sites. In this particular case we have chosen the Mn core spin to align with one of the (100) crystal axes (which is the bulk easy axis [28]). As a result, the spectra at the four nearest-neighbor As sites are identical due to the residual symmetry operations of C_2 and S_4 about the crystal axes. The twelve second-nearest-neighbor Ga sites are divided into two classes with four and eight sites each. The acceptor states are almost fully spin-polarized (parallel to the Mn core spin) and split into three energy levels due to the spin-orbit interaction. For bulk n -doped $\text{Ga}_{1-x}\text{Mn}_x\text{As}$ the Fermi level lies above the upper acceptor state, so the impurity is ionized and all three levels would be visible in a tunneling experiment. If the Fermi level lies below the upper acceptor state, such as in bulk p -doped $\text{Ga}_{1-x}\text{Mn}_x\text{As}$, then due to the electron-electron interaction only one localized state

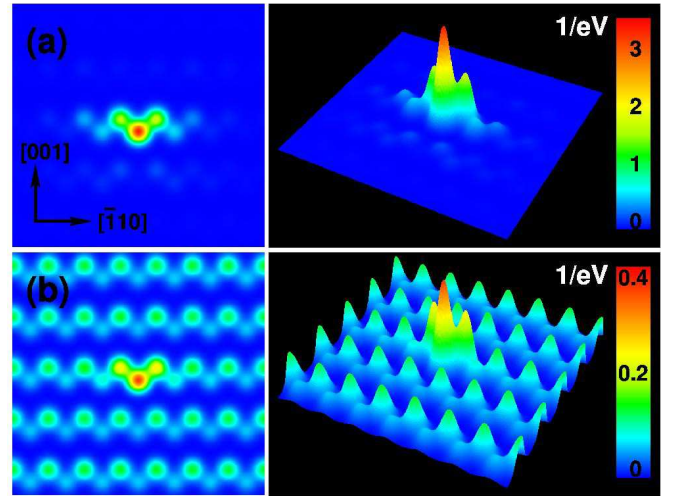


FIG. 2: (color) The spatial structure of (a) the Mn acceptor level at 113 meV and of (b) the valence band LDOS at -500 meV. The LDOS peaks are centered at the Mn atom, and are extended mainly on the (001) plane. In (b), far away from the Mn site, the sites with higher LDOS are occupied by the As atom, and with lower LDOS are occupied by the Ga atom. We have assumed that the squared modulus of the Wannier functions to be a Gaussian with a width of half the distance between neighboring Ga and As atoms.

will be visible above the Fermi level and none below. Due to band-bending at the surface it is often possible to see both the ionized and neutral dopants in the same sample (as in Ref. 21). As the Mn core spin rotates, the orbital character of the acceptor states changes, but the three energy levels remain the same within the sp^3 model. There is some experimental evidence for the existence of the two additional acceptor energy levels [29]. The significant enhancement of the spin-up LDOS continues into the valence band to 1.5 eV below the band edge. The spin-polarized resonances emerge at an energy close to the split-off band top (~ 350 meV below the band edge). On the other hand, the spin-down band is weakly perturbed and non-resonant. Figure 1 (c) and (d) also show that the large enhancement of the valence band LDOS extends to the second-nearest neighbors. From the spectral weight of the acceptor state, $\sim 5\%$ at each As site, we estimate the p - d exchange interaction βN_0 to be $\frac{2}{5}U_1 \times 20\% \approx -0.3$ eV, within a factor of 3 of that obtained from transport measurements (see Chapter 1 in Ref. 6). The discrepancy may come from the enhanced LDOS near the Mn spin, which is not included in the transport modeling.

The spatial structure of the LDOS is further illustrated in Fig. 2. For the Mn potential used here, the upper acceptor state is peaked at the Mn site. The ratio between the peak heights at the Mn and at the nearest-neighbor As sites is related to the strength of U_0 and U_1 . Generally, increasing the potential strength at one site re-

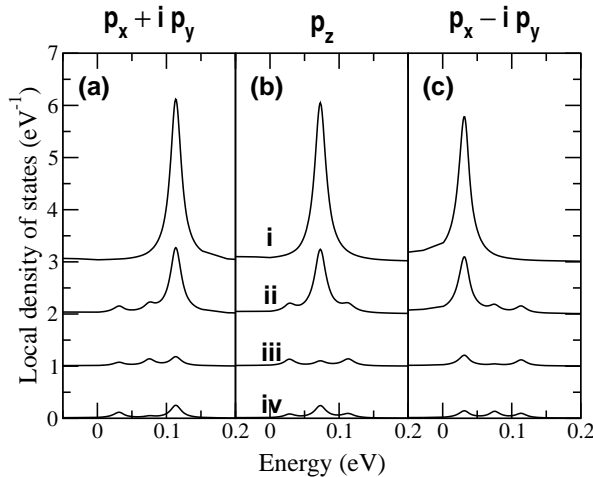


FIG. 3: The orbitally resolved LDOS for (a) $p_x + ip_y$, (b) p_z and (c) $p_x - ip_y$ orbitals. The Mn core spin is aligned with the z -axis. Each panel contains four LDOS curves. From top to bottom, the curves show the LDOS at (i) the Mn, (ii) the nearest-neighbor (As) sites, and (iii) and (iv) the second-nearest-neighbor (Ga) sites. Cases (iii) and (iv) correspond to the configurations (c) and (d) in Fig. 1 respectively. The LDOS spectra are shifted by multiples of one unit for easier visualization.

duces the spectral weight at the same site. The degree of acceptor-state localization apparent in Fig. 2 is determined largely by the effective band masses of the GaAs host, which are dependent on the tight-binding parameters of Ref. 27. If the spin is aligned with the z axis, the uppermost acceptor state is spatially extended in the x - y plane, because the orbital character, shown in Fig. 3, is $p_x + ip_y$.

We also calculate the LDOS for two nearby Mn dopants by inverting the Dyson equation for a two-impurity potential. When the two Mn core spins are parallel, the acceptor states centered at the two Mn sites interfere, and further split into “bonding” and “antibonding” states. When the two Mn core spins are antiparallel, one of the U_1 terms acts on spin-down As-orbitals, and the potential for the spin-up (down) states at one Mn site is the same as for the spin-down (up) states at the other Mn site. Therefore, the acceptor states remain in three degenerate levels. The splitting of the acceptor level for two parallel Mn core spins can be used as a probe for the range of interaction between Mn dopants. Figure 4 shows the long-ranged nature of the interaction. It also shows the anisotropy of the interaction resulting from the spin-orbit interaction. Because the acceptor state has an orbital character more extended in the plane perpendicular to the Mn core spin, the splitting of the acceptor level is the largest when the Mn core spins are oriented perpendicular to the axis that joins them.

In summary we have presented calculations of the LDOS near Mn in GaAs. The p - d hybridization in-

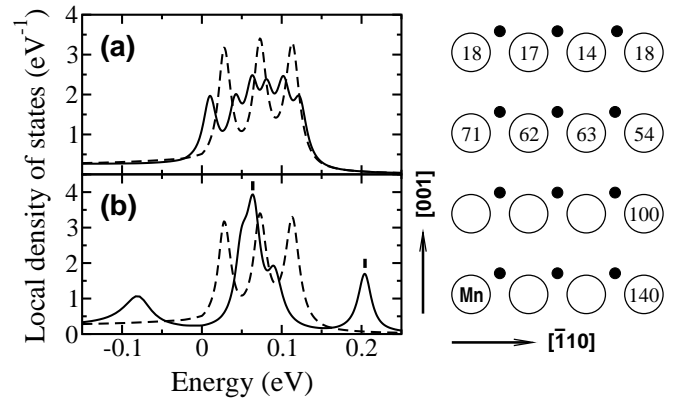


FIG. 4: Splitting of the acceptor levels. The left panel shows the spectra at the Mn site with two Mn dopants separated by (a) $(0, 0, 3)$ and (b) $(-3/2, 3/2, 0)$. The dashed line shows the spectrum when there is only one Mn dopant. In (b) the two split peaks of the 113 meV level are indicated by the two heavy-line segments. The right panel shows the amount of the splitting of the 113 meV level. One of the Mn atoms is located at the $(0, 0, 0)$ site (bottom-left corner), and the other is at one of the circles. The number in the circle shows the splitting energy in meV. Both Mn core spins are aligned with the z -axis. The black dots show the As sites.

duces spin-polarized resonances that enhance the LDOS near the valence band edge. The spin-orbit interaction splits the acceptor level, and introduces anisotropy to the Mn-Mn interaction in addition to the crystal anisotropy. The range of the Mn-Mn interaction is shown to extend through several lattice constants. For quantitative comparisons with STS measurements, significant surface effects are expected for a Mn atom at the top layer because the Mn atom has one less As neighbor, and the hybridization changes. However, it has been reported that dopant atoms as deep as in the fifth layer are seen by STS [21], and the spectra for these cases should closely resemble the bulk.

This work was supported under the ARO MURI DAAD19-01-1-0541.

- [1] H. Munekata *et al.*, Phys. Rev. Lett. **63**, 1849 (1989).
- [2] H. Ohno *et al.*, Phys. Rev. Lett. **68**, 2664 (1992).
- [3] G. A. Medvedkin *et al.*, Jpn. J. Appl. Phys. **39**, L949 (2000).
- [4] M. L. Reed *et al.*, Appl. Phys. Lett. **79**, 3473 (2001).
- [5] S. Sonoda *et al.*, J. Cryst. Growth **237**–**239**, 1358 (2002).
- [6] *Semiconductor Spintronics and Quantum Computation* D. D. Awschalom, N. Samarth, and D. Loss, eds., (Springer Verlag, Heidelberg, 2002).
- [7] S. A. Wolf *et al.*, Science **294**, 1488 (2001).
- [8] F. Matsukura *et al.*, Phys. Rev. B **57**, R2037 (1998).
- [9] J. Szczytko *et al.*, Phys. Rev. B **59**, 12935 (1999).
- [10] B. Beschoten *et al.*, Phys. Rev. Lett. **83**, 3073 (1999).
- [11] H. Ohno *et al.*, Nature (London) **408**, 944 (2000).

- [12] Y. Nagai *et al.*, Jpn. J. Appl. Phys. **40**, 6231 (2001); E. J. Singley *et al.*, Phys. Rev. Lett. **89**, 097203 (2002).
- [13] T. Dietl *et al.*, Science **287**, 1019 (2000).
- [14] T. Dietl, A. Haury, and Y. M. d'Aubigné, Phys. Rev. B **55**, R3347 (1997).
- [15] H. Akai, Phys. Rev. Lett. **81**, 3002 (1998).
- [16] J. Okabayashi *et al.*, Phys. Rev. B **64**, 125304 (2001).
- [17] S. Sanvito, P. Ordejón and N. A. Hill, Phys. Rev. B **63**, 165206 (2001).
- [18] M. van Schilfgaarde and O. N. Mryasov, Phys. Rev. B **63**, 233205 (2001).
- [19] M. E. Flatté and D. E. Reynolds, Phys. Rev. B **61**, 14810 (2000).
- [20] G. Zaránd and B. Jankó, Phys. Rev. Lett. **89**, 047201 (2002).
- [21] R. M. Feenstra *et al.*, Phys. Rev. B **66**, 165204 (2002).
- [22] P. Vogl and J. M. Baranowski, Acta. Phys. Polo. **A67**, 133 (1985).
- [23] T. Dietl, F. Matsukura, and H. Ohno, Phys. Rev. B **66**, 033203 (2002).
- [24] G. F. Koster and J. C. Slater, Phys. Rev. **95**, 1167 (1954).
- [25] H. P. Hjalmarson *et al.*, Phys. Rev. Lett. **44**, 810 (1980).
- [26] J.-M. Tang and M. E. Flatté, Phys. Rev. B **66**, 060504(R) (2002); M. E. Flatté and J. M. Byers, in *Solid State Physics*, edited by H. Ehrenreich and F. Spaepen (Academic Press, New York, 1999), vol. 52, pp. 137–228.
- [27] D. J. Chadi, Phys. Rev. B **16**, 790 (1977).
- [28] H. X. Tang *et al.*, Phys. Rev. Lett. **90**, 107201 (2003).
- [29] T. C. Lee and W. W. Anderson, Solid State Commun. **2**, 265 (1964).